JOURNAL OF MATERIALS SCIENCE 29 (1994) 2767–2774

Stress analysis of elastomeric materials at large extensions using the finite element method

Part III *Coalescence of primary and secondary cracks and generation of fracture surface roughness*

Y. FUKAHORI, W. SEKI
Research and Development Division, Bridgestone Corporation, Kodaira-shi, Tokyo 187, Japan

A newly developed finite element method is applied to the stress and strain analyses of stress fields, at the vicinity of a primary crack surrounded by secondary cracks. The results show that the primary crack propagation deviates from the crack axis, when a secondary crack entered the stress fields of the primary crack within the distance of the diameter of the secondary crack. The fundamental unit of surface roughness, the deviation from planarity, will be the diameter of the secondary crack. The roughness generated in real elastomers strongly depends on mechanical hysteresis, and thus the fracture surface energy of the materials.

1. Introduction

In a series of studies [1, 2], we have performed stress and strain analyses around spherical holes and rigid spherical particles in elastomeric materials under large deformation, using a newly developed finite element method. The results obtained are of great importance not only to the initiation of microcracks, which arise from such inclusions in the matrix, but also for the propagation of cracks passing through the coalescence of microcrack to microcrack and microcrack to macrocrack.

For a single crack in a homogeneous matrix, the fracture surface generated by the propagation of a crack will generally show a perfect planarity, because the crack propagates in a straightforward fashion, following the maximum stress produced in the vicinity of the crack, perpendicular to the extension direction. According to the Griffith concept, the work done during fracture should be increased for the generation of a concave–convex surface compared with that of plane surface, because more energy should be expended for creating the increased surface area. This means that when we face the rough fracture surface of materials, we can assume that the fracture took place in a material of high fracture surface energy (i.e. of high fracture toughness).

Nearly 15 years ago, Fukahori [3] and Fukahori & Andrews [4] found an inverse correlation between fracture surface roughness, R and mechanical hysteresis ratio, h in highly deformable materials such as rubber, i.e. $R \times h =$ constant. As h increases, the fracture surface energy T also increases, as described by Andrews' equation [5]; the above relation also gives the inverse correlation between the fracture surface roughness, R and the fracture surface energy, T. This result contrasts with that expected from the Griffith concept, thus it was proposed [3, 4] that the mechanism of roughness generation in visco-elastic solids is based on the hypothesis that surface roughness (i.e. a deviation of the fracture from perfect planarity) is generated through the coalescence of a primary crack and secondary cracks. Secondary cracks such as cavities, voids and particles propagate in the high-stress region surrounding a primary crack front and join up with the primary crack, even though they lie in a different plane from the path of the primary crack, by shear of the intervening material. When we consider the growth of a secondary crack in non-linear visco-elastic materials, the energy required to propagate a crack increases with fracture surface energy, T, of the material. Alternately, in a given stress field a secondary crack will only propagate in a small zone surrounding a primary crack if T is large, because the stress level decays with distance from the primary crack tip. As the scale of roughness will directly relate to the separation of the planes of the primary and secondary cracks, a higher fracture surface energy will produce a lower degree of roughness. These situations are summarized in the literature [6]. The heavy and complex roughness seen on the fracture surface of elastomers, which may be in the order of 1 mm, can be understood only when we consider the stress fields consisting of a primary crack and surrounding secondary cracks and their coalescence, instead of the propagation of a single crack.

In recent years, many studies [7–9], have been carried out on the ductile fracture of metals, in which the microcracking around the tip of a macrocrack is discussed in relation to nucleation, propagation and coalescence of microvoids, microcracks and macrocracks. For this purpose, a finite element method is used to estimate the fracture process of a propagating crack. In previous papers [1–2], we applied a newly developed finite element method to stress and strain analyses around spherical holes and spherical rigid particles in elastomers. The results thus obtained show

0022–2461

that stress and strain distribution around such inclusions deviate from the theoretical solution, as the average strain increases and as the nonlinearity of matrix elastomers increases.

In the present report the process by which a primary crack develops and joins up to a secondary crack, and generates a fracture surface roughness in nonlinear elastomeric materials, is discussed. This study deals with problems of microcracking of elastomers under static loading, which will make analysis of dynamic fracture possible in the near future.

2. Finite element methods and experiments

As theoretical backgrounds of a finite element method (FEM) have already been described in detail in previous papers [1,2], a brief outline of the newly developed FEM is given here. The method includes two important elements. Firstly, the strain energy function of real elastomers, the elastic energy stored in a deformed body, is experimentally evaluated through strip bi-axial (pure shear) testing. Secondly, computer programming has been improved based on the mixed variational method to treat the problems of incompressibility in elastomers.

In this study, two-dimensional simulation (plane strain condition) is performed to give finer meshes for computation and thus more accurate results. The strain energy function of slightly filled natural rubber (NR2) is used for simulation.

The secondary crack is located in front of the primary crack under large extension, and a specimen of dimensions schematically illustrated in Fig. 1 is fixed to hard clamps and extended perpendicular to the primary crack axis X. The secondary crack is assumed to have a radius of r_0, equal to the curvature of the primary crack, and to approach the primary crack from the angle of 45° to the X-axis (example 1; Fig. 2a) and parallel to the X-axis keeping the distance $Y = r_0$ (example 2; Fig. 2b).

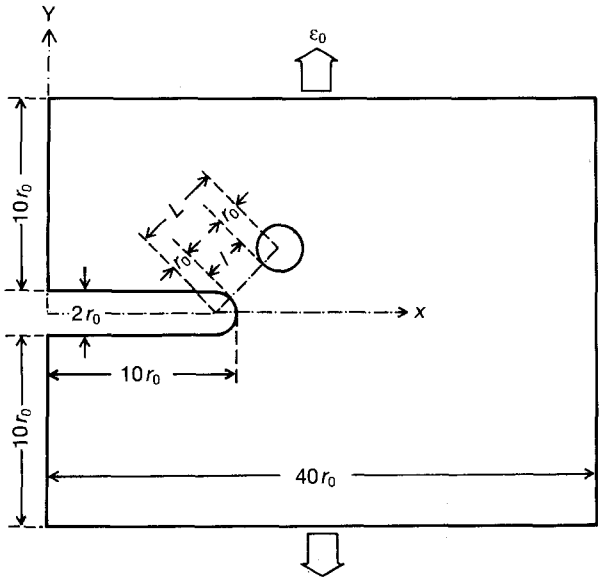

Figure 1 Finite-element model of a primary crack of length $10r_0$ and tip curvature r_0, and a secondary crack of radius r_0 subjected to a uniform gross strain ε_0.

The distance between the centres of curvature of two cracks, L $(= l + 2r_0)$ where l is the minimum distance between the surfaces of two cracks, is varied in both cases. The tip of the primary crack and the circumference of the secondary crack are divided equally and named $P_1 \sim P_5$ and $S_1 \sim S_5$, respectively, as shown in Fig. 3. Fig. 4 is an example of finite element models when the primary and secondary cracks are adjacent. Stress and strain are predicted by the maximum principal stress (true stress) σ and the maximum principal strain ε. Uniform (average) strain ε_0 is applied to the system remote from the cracks. Stress and strain distributions are represented on the undeformed coordinates.

3. Results and discussion

3.1. Stress and strain distribution around primary and secondary cracks

Figs 5 and 6 are distorted meshes, originally given in Fig. 4, at average strains of 10 and 100%, respectively.

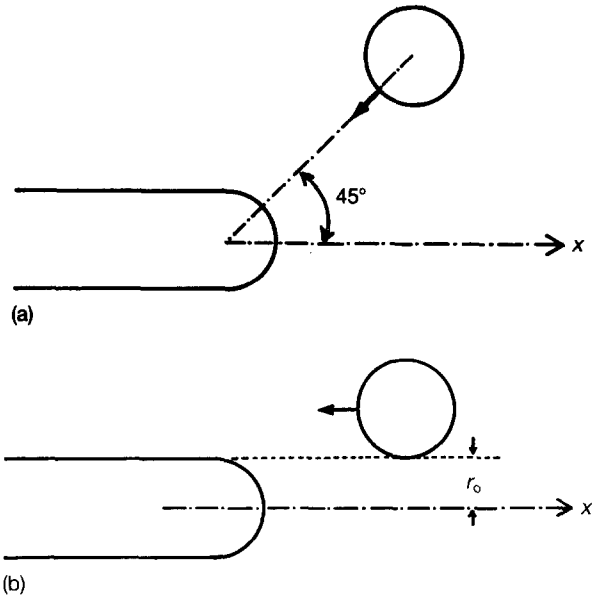

Figure 2 (a) Schematic illustration representing the situation of a secondary crack approaching a primary crack from the angle of 45° to the X-axis (example 1). (b) As (a), approaching parallel to the X-axis keeping the distance $Y = r_0$ (example 2).

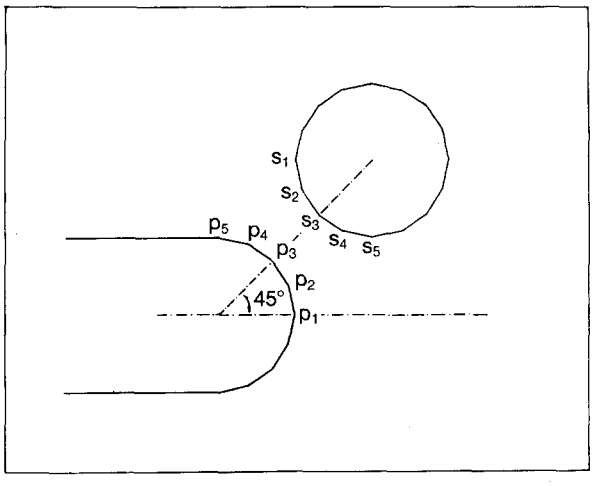

Figure 3 Equally divided crack fronts.

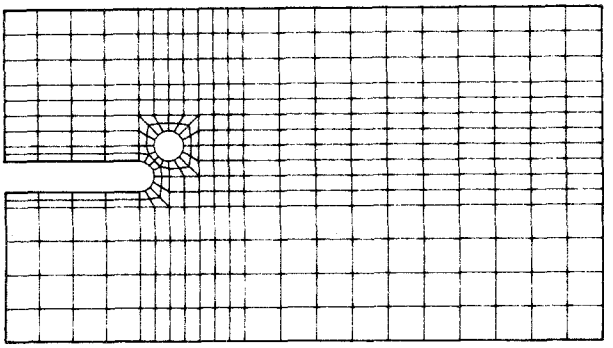

Figure 4 An example of finite element meshes.

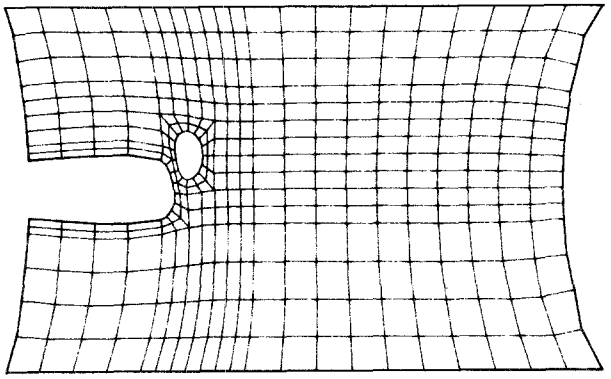

Figure 5 A distorted mesh at $\varepsilon_0 = 10\%$.

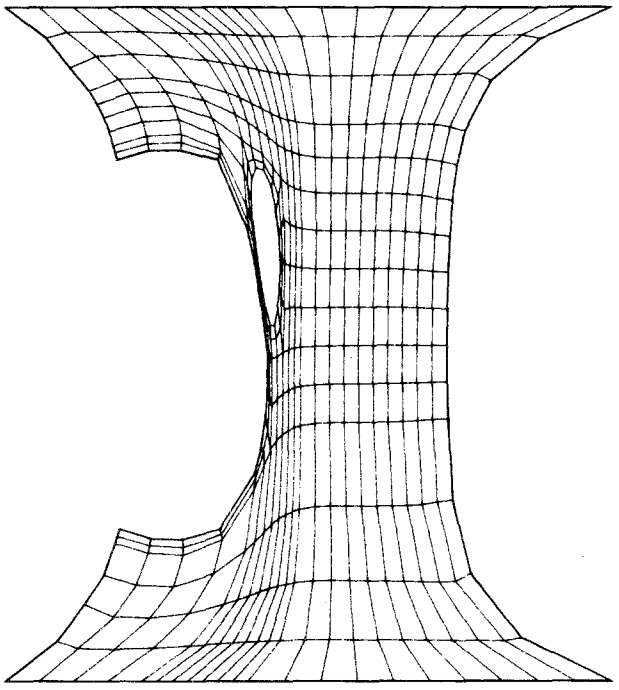

Figure 6 A distorted mesh at $\varepsilon_0 = 100\%$.

Figs 7 and 8 are the stress and strain distributions in the vicinity of the tip of a primary crack at $\varepsilon_0 = 100\%$ when a primary crack alone exists. The maximum stress and strain occur at point P_1 as the maximum stress and strain occur at point S_1 in a single secondary crack. Fig. 9 shows the stress distribution around the tip of a primary crack when the secondary crack is

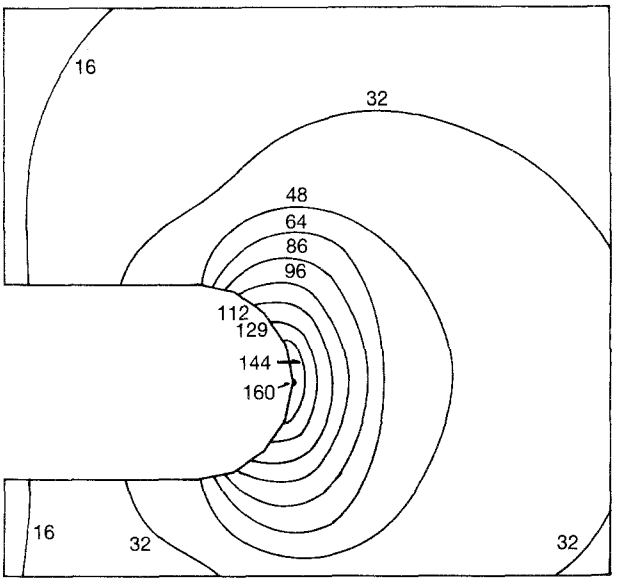

Figure 7 Contour map of the maximum principal stress (10 MPa) in the vicinity of the tip of a primary crack at $\varepsilon_0 = 100\%$.

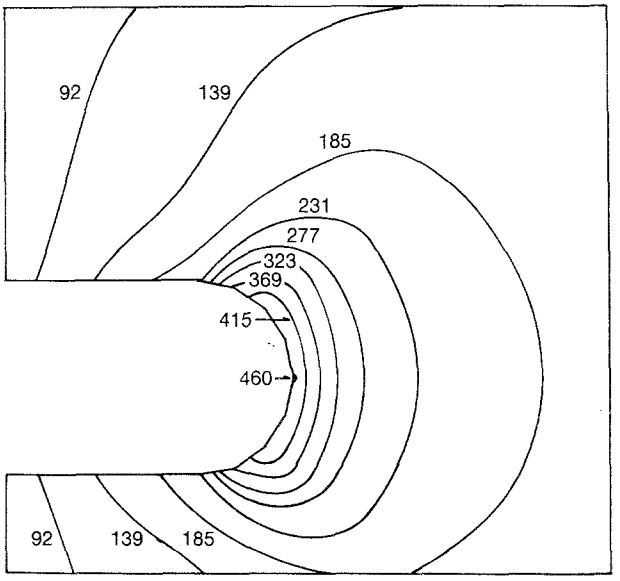

Figure 8 Contour map of the maximum principal strain (10 MPa) in the vicinity of the tip of a primary crack at $\varepsilon_0 = 100\%$.

at a distance, $l/2r_0 = 0.41$ in example 1 at $\varepsilon_0 = 100\%$. It is clearly seen that the position at which the maximum local stress occurs deviates from P_1 to P_3 at the tip of the primary crack, and from S_1 to nearly S_3 at the circumference of the secondary crack. Similarly, the maximum local strain appears at points P_2 and S_2 deviated from P_1 and S_1, as shown in Fig. 10. Figs 11 and 12 show two cracks that are much closer, i.e. $l/2r_0 = 0.061$ and at $\varepsilon_0 = 100\%$. The maximum local stress and strain around two cracks occur at P_3 and S_3, and their magnitudes are much higher than those given when both cracks remain undisturbed by each other.

3.2. Deviation of the trajectory of crack propagation from planarity

In Fig. 13 the maximum principal strain at points $P_1 \sim P_5$ is plotted as a function of the normalized

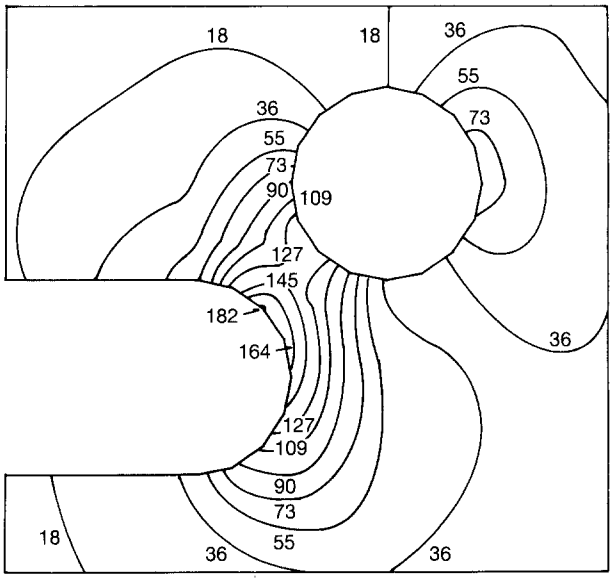

Figure 9 Contour map of the maximum principal stress (10 MPa) around the tip of the primary and secondary cracks at $l/2r_0 = 0.41$ and $\varepsilon_0 = 100\%$ (example 1).

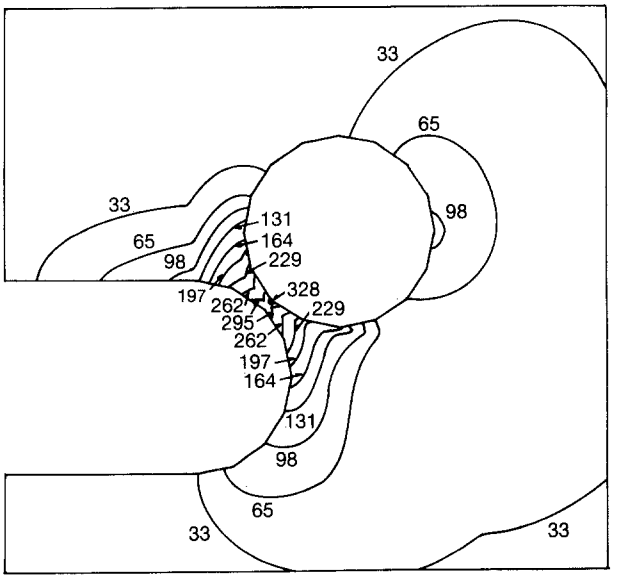

Figure 11 Contour map of the maximum principal stress (10 MPa) around the tip of the primary and secondary cracks at $l/2r_0 = 0.061$ and $\varepsilon_0 = 100\%$ (example 1).

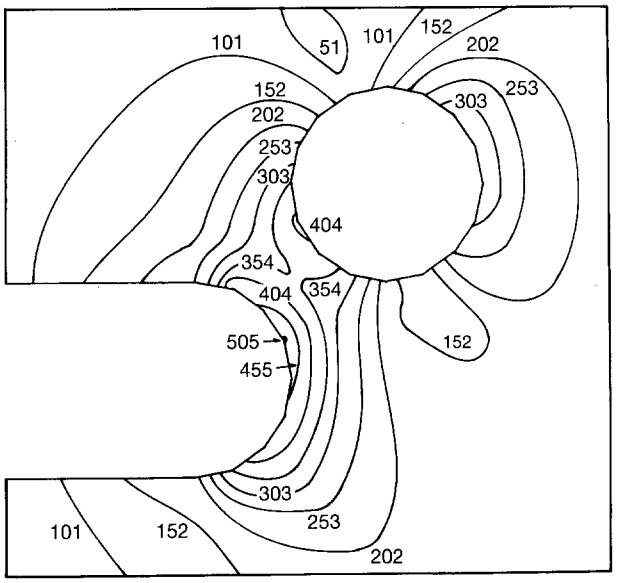

Figure 10 Contour map of the maximum principal strain (10 MPa) around the tip of the primary and secondary cracks at $l/2r_0 = 0.41$ and $\varepsilon_0 = 100\%$ (example 1).

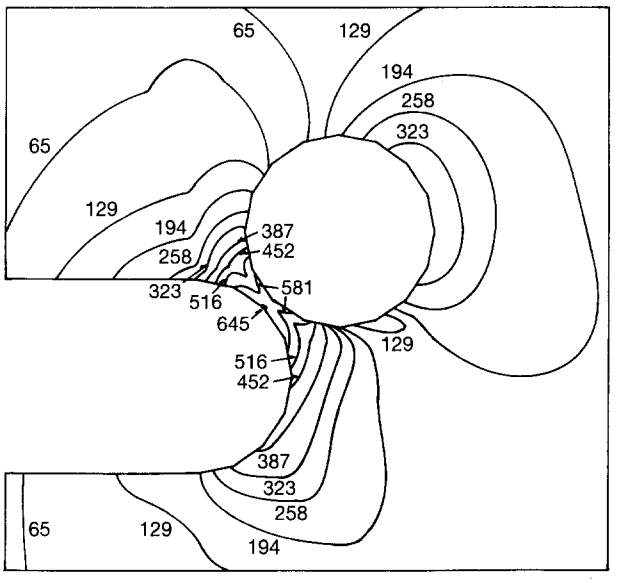

Figure 12 Contour map of the maximum principal strain (10 MPa) around the tip of the primary and secondary cracks at $l/2r_0 = 0.061$ and $\varepsilon_0 = 100\%$ (example 1).

distance $l/2r_0$, keeping the angle of 45° (example 1) at $\varepsilon_0 = 150\%$. It is shown that the maximum local strain which appears around the primary crack changes its position from P_1 to P_2 and to P_3 as the distance decreases. At the same time, the position of the maximum local strain at the circumference of the secondary crack also varies from S_1 to S_3 with decreasing distance, as shown in Fig. 14. In both cases (Figs 13 and 14) the position of the maximum local strain deviates from P_1 and S_1 to other points, i.e. from the crack axis X when $l/2r_0 \leqq 1$. The same situations are also seen in example 2. When the secondary crack approaches the primary crack parallel to the X-axis, keeping $Y = r_0$, the position of the maximum local strain deviates from P_1 and S_1 to other points at $l/2r_0 \leqq 1$, as shown in Figs 15 and 16.

It is concluded that when the secondary crack enters the stress fields of the primary crack within the distance $l/2r_0 = 1$, i.e. the diameter of the secondary crack, the position of the maximum local strain (and thus the maximum local stress) at the boundary of primary and secondary cracks varies from P_1 and S_1 to other points.

As a crack initiates and propagates at a point where the maximum local stress or strain occurs in the system, then the primary crack deviates from the X-axis when it reaches the secondary crack within the distance of the diameter of the secondary crack. However, it seems that it is when the position of the maximum local strain in the primary and secondary cracks lie at P_2–P_3 and S_2–S_3, respectively (i.e. $l/2r_0 \fallingdotseq 1/2$, when $l = r_0$) that two cracks face and coalesce each other.

Therefore the fundamental unit of roughness, ΔR, the deviation from the planarity, will be given by the summation of the radius of two cracks, $2r_0$ and the

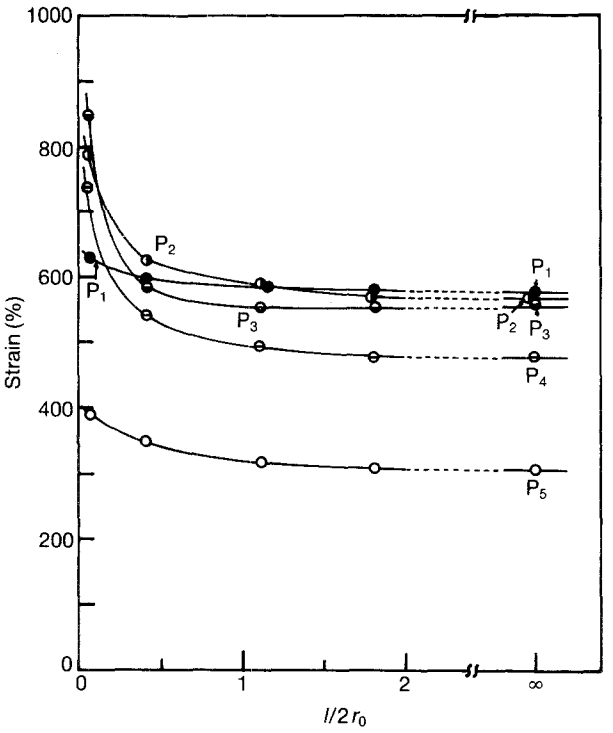

Figure 13 Maximum principal strain at points P_1–P_5 as a function of the normalized distance $l/2r_0$ at $\varepsilon_0 = 150\%$ (example 1).

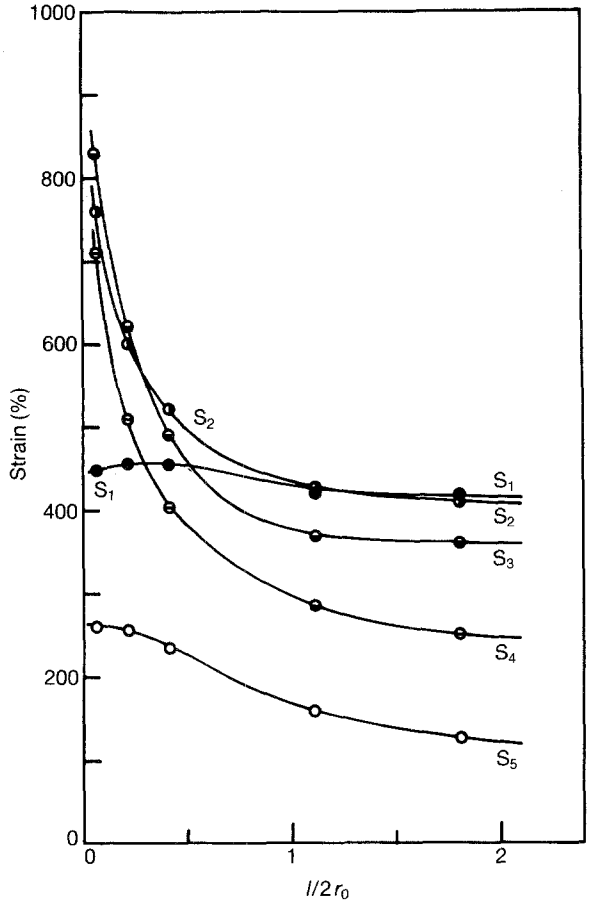

Figure 14 Maximum principal strain at points S_1–S_5 as a function of the normalized distance $l/2r_0$ at $\varepsilon_0 = 150\%$ (example 1).

distance between two cracks, r_0, considering the angle to the X-axis, which is nearly the diameter of the secondary crack propagated before the coalescence with the primary crack. These situations are shown schematically in Fig. 17, which also shows slippage of the crack axis.

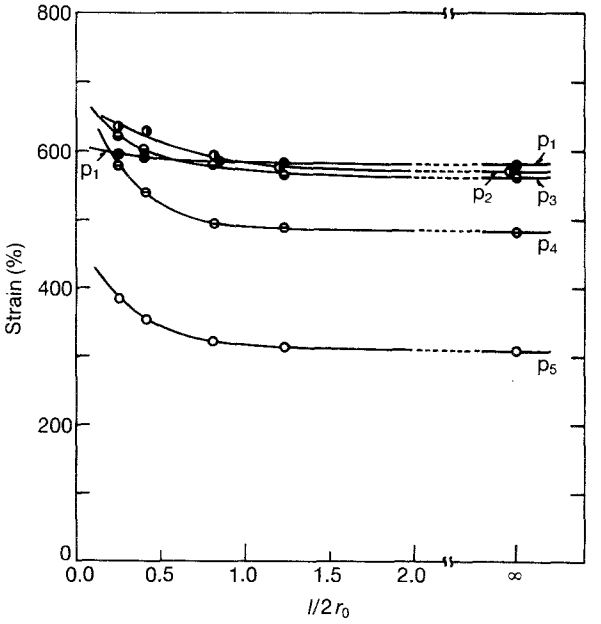

Figure 15 Maximum principal strain at points P_1–P_5 as a function of the normalized distance $l/2r_0$ at $\varepsilon_0 = 150\%$ (example 2).

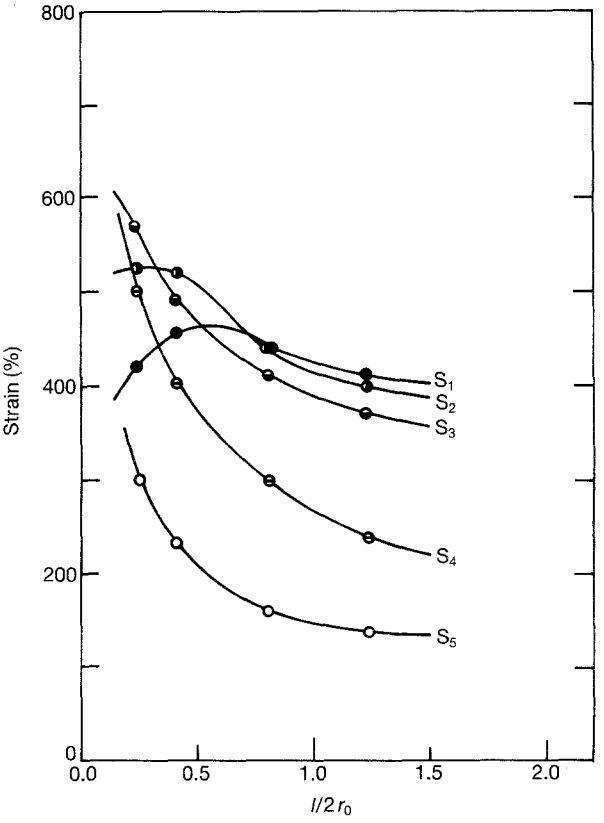

Figure 16 Maximum principal strain at points S_1–S_5 as a function of the normalized distance $l/2r_0$ at $\varepsilon_0 = 150\%$ (example 2).

3.3. Factors in governing the surface roughness formation

Fig. 18 shows the trajectory of a primary crack propagated and coalescence with cavities, indicating that the deviation from the crack axis strongly depends on the number and size of cavities. Figs 19a, b and 20a, b are fracture surfaces of unifilled Styren Butadien Rubber (SBR) and carbon black-filled SBR vulcanizates, respectively, whose features are quite different (i.e. very

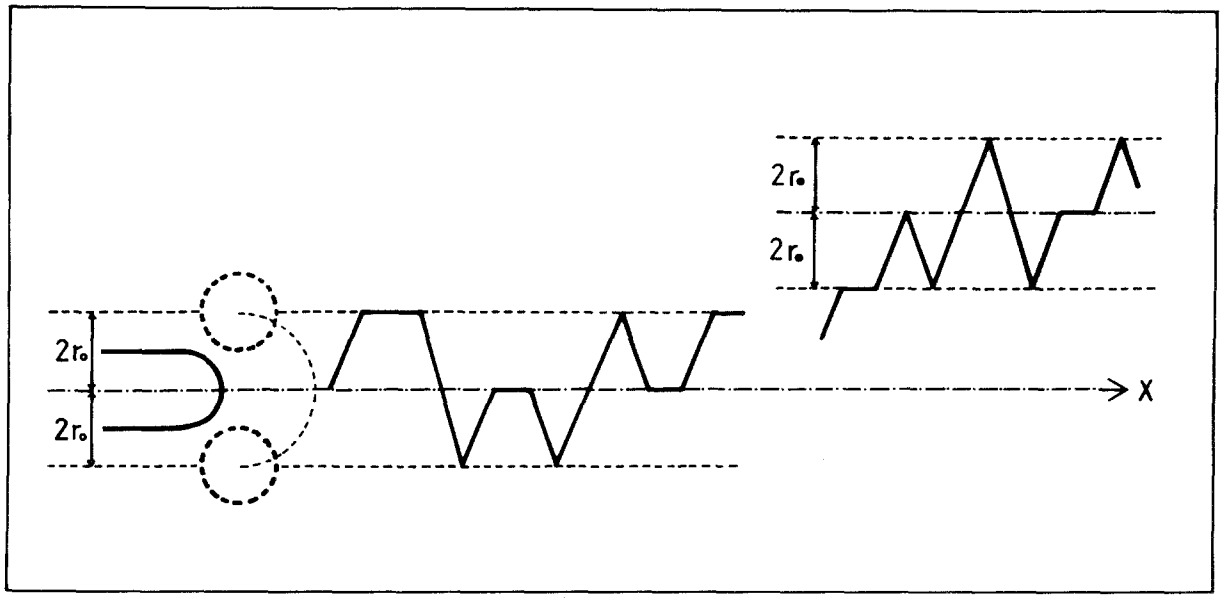

Figure 17 Fundamental unit of the roughness, $\Delta R = \pm 2r_0$ and the slippage of the crack axis (schematic).

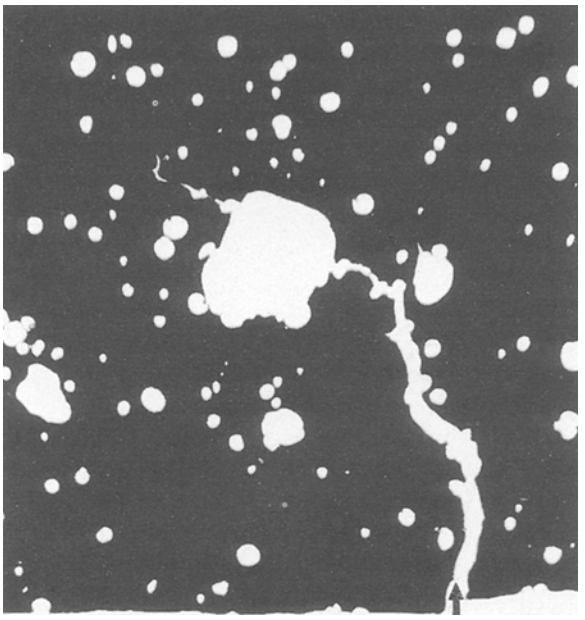

Figure 18 Photographs showing the coalescence of the primary crack and cavities.

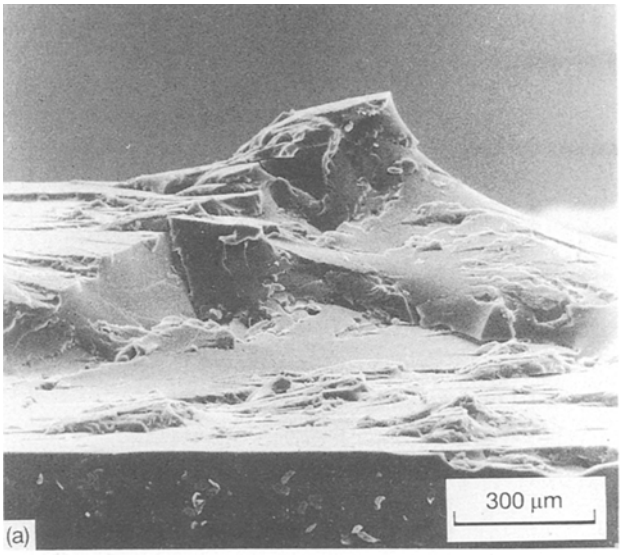

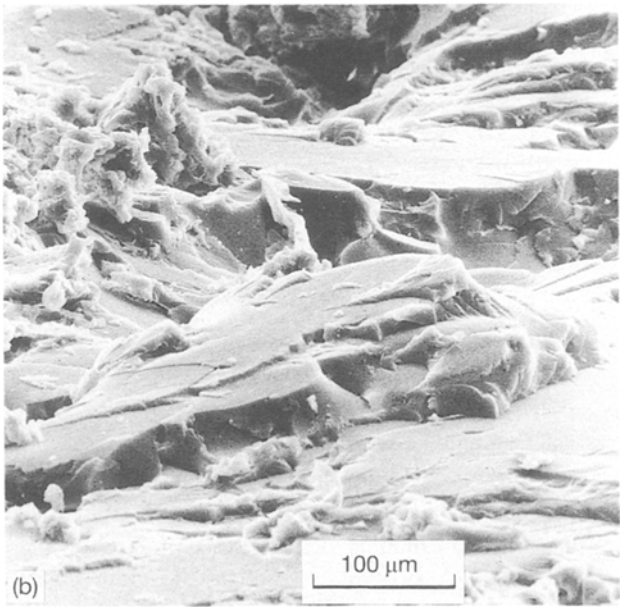

Figure 19 (a) Three-dimensional picture of a fracture surface of unfilled SBR. (b) As (a) but at higher magnification.

rough in the former and very smooth in the latter). The maximum roughness is of the order of 50 μm in filled SBR and of ~ 300–500 μm in unfilled SBR. The compounding recipe and their physical properties are given in Table I and Fig. 21.

Now we consider the factors to govern the surface roughness formation in two rubber vulcanizates. Firstly, we must consider whether there is a large difference in the number or size of inherent flaws in the two materials. Although there is little detailed information available about the number of inherent flaws in rubber vulcanizates, it is likely that there is no large difference between unfilled and filled rubbers. However, the number is probably smaller in unfilled rubber than in filled rubber, considering the poor dispersion of carbon blacks in rubber compounds. On the other hand, many studies [10–13] have been

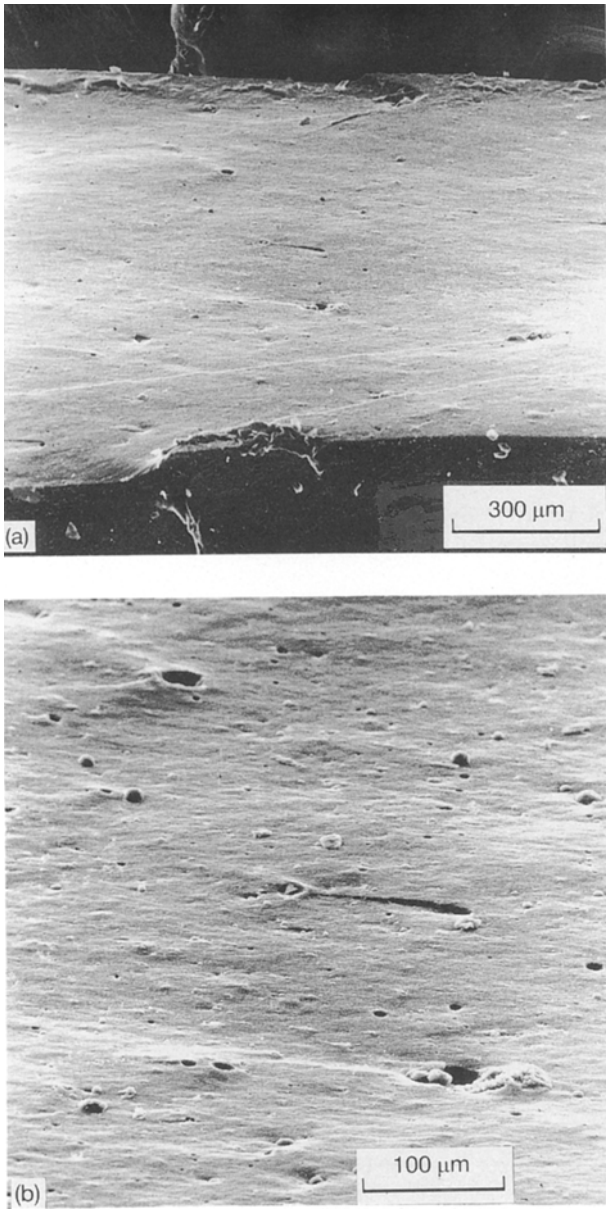

Figure 20 (a) Three-dimensional picture of a fracture surface of filled SBR. (b) As (a) but at higher magnification.

TABLE I Compounding details of materials (parts by weight) and their physical properties

	Unfilled SBR	Filled SBR
SBR	100	100
HAF Carbon	0	50
Surphur	1.5	1.5
Hysteresis ratio, h_{100}	0.157	0.424
Fracture energy, W_0, (MJ m^{-3})	5.60	47.8

reported for the inherent flaw size of Co in rubbers, which shows that values of Co are almost independent of species of rubbers and whether they are unfilled or filled, being of the order of $\sim$ 40–60 μm. Accordingly, a very large difference in surface roughness in the two rubbers (shown in Figs 19 and 20) is not attributable to the number or size of inherent flaws originally involved in the material.

As a second step, we must consider the propagation of inherent flaws (as secondary cracks) before their

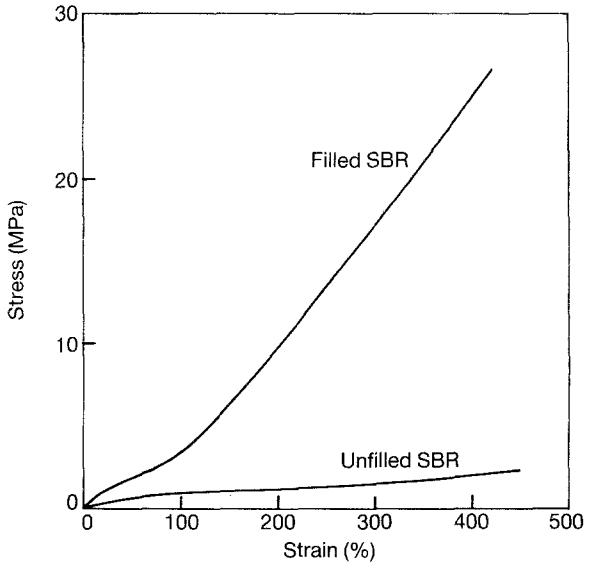

Figure 21 Stress–strain curves in simple tension.

coalescence with the primary crack. The important point for the coalescence of the primary and secondary cracks is the effective number and the effective size of secondary cracks, which have propagated in the strong stress field around the primary crack when two cracks coalesce. The roughness of nearly 50 μm in filled SBR, as given in Fig. 20, shows that secondary cracks had grown slightly only in the vicinity of the crack axis X when they coalesced with the primary crack. On the other hand, in unfilled SBR (as shown in Fig. 19) the very rough fracture surface (whose minimum roughness is nearly 50 μm but maximum is of the order of 300–500 μm) means that secondary cracks grew largely even in the stress field far from the original crack axis.

It is natural that the speed of crack propagation strictly depends on the fracture surface energy T of the matrix rubber, i.e. the higher the fracture surface energy, the lower the propagation of the crack. The physical properties of unfilled and filled SBR are shown in Fig. 21 and Table I. The mechanical hysteresis ratio, h and the fracture energy, W_0 given by the area under the stress–strain curve (and thus T) are much higher in filled than in unfilled SBR. Therefore, as Fukahori & Andrews [3, 4] have shown previously, in a given stress field surrounding the primary crack, inherent flaws (then secondary cracks) in unfilled SBR will propagate much faster and in a much larger zone surrounding the primary crack than in filled SBR, which as a result, generates a very rough fracture surface in unfilled SBR.

4. Conclusion

A newly developed finite element method is applied to the stress and strain analysis of stress fields at the vicinity of a primary crack surrounded by secondary cracks. The results show that the primary crack propagation deviates from the crack axis when a secondary crack enters the stress fields of the primary crack, within the distance of the diameter of the secondary crack. The fundamental unit of surface

roughness, the deviation from planarity, will be the diameter of the secondary crack. The roughness generated in real elastomers depends heavily on mechanical hysteresis and thus the fracture surface energy of the materials, as shown by Fukahori & Andrews [3, 4]. In a given stress field surrounding the primary crack, inherent flaws (then secondary cracks) in unfilled SBR (of a small T) will propagate much faster, and in a much larger zone surrounding the primary crack, than in filled SBR (of a large T), which as a result generates a very rough surface in unfilled SBR.

References

1. Y. FUKAHORI and W. SEKI, *J. Mater. Sci.* **28** (1993) 4143.
2. Y. FUKAHORI and W. SEKI, *J. Mater. Sci.* **28** (1993) 4471.
3. Y. FUKAHORI, PhD thesis, University of London, 1976
4. Y. FUKAHORI, and E. H. ANDREWS, *J. Mater. Sci* **13** (1978) 777.
5. E. H. ANDREWS, *J. Mater. Sci.* **9** (1974) 887.
6. Y. FUKAHORI, in "Fractography of Rubbery Materials" edited by A. N. Bhowmick and S. K. De (Elsevier, London, New York, 1991) p.71.
7. V. TVERGAARD and A. NEEDLEMAN, *Acta Met.* **32-1** (1984) 157.
8. N. ARAVAS and R. M. MCMEEKING, *J. Mech. Phys. Solids* **33** (1985) 25.
9. H. KITAGAWA and S. KOMEDA, *Proc. Int. Conf. Computational Mech.* **5** (1986) 157.
10. J. P. BERRY, *J. Polym. Sci.* **50** (1961) 313.
11. A. N. GENT, in "Science and Technology of Rubber" edited by F. R. Eirich (Academic Press, New York, 1978) p. 419.
12. G. R. HAMED, *Rubb. Chem. Tech.* **56** (1983) 244.
13. Y. FUKAHORI, *Nippon Gomu Kyokai Shi (Jpn)* **58** (1985) 625.

Received 4 September 1992
and accepted 27 September 1993